

Tracer Experiments within Composite Soil Column Investigated by MRI

VLADIMÍRA JELÍNKOVÁ^{1,2}, MILENA CÍSLEROVÁ¹, ANDREAS POHLMEIER²
and DAGMAR VAN DUSSCHOTEN²

¹Department of Irrigation, Drainage and Landscape Engineering, Faculty of Civil Engineering,
Czech Technical University in Prague, Prague, Czech Republic; ²Research Centre Jülich,
Institute of Chemistry and Dynamics of the Geosphere (ICG), Jülich, Germany

Abstract: The magnetic resonance imaging (MRI) technique was used for the visualisation and interpretation of flow paths. A set of tracer-infiltration experiments was performed on soil columns filled with packed homogeneous sand and with a composite sand-soil system. The flow paths were visualised using a tracer-solution containing $\text{Ni}(\text{NO}_3)_2$ which is characterised by relaxation times different from that of the infiltrating water. The tracer pulse was added under hydraulic steady state conditions. Small disturbances in the tracer front were observed during the breakthrough in the case of a homogeneous sample. More pronounced effects were seen with the composite sample. The vertical components of the velocity fields were evaluated for the experiments presented. The irregularities in the tracer front and in the velocity fields were in this case attributed to the preferential flow phenomena in combination with air bubble entrapment. Beside that, two consecutive tracer pulses were performed with the aim of testing the potential influence of the different solute concentrations on the adsorption power. Both concentrations had negligible impacts on the acquired image. The presented results are constrained by the limits of the described technology; further investigations are being carried out using more advanced equipment.

Keywords: Cambisol; infiltration; laboratory experiments; magnetic resonance imaging; porous medium; preferential flow; sand; soil samples; tracer; velocity field

In the last few decades, noninvasive imaging methods, such as Computed Tomography (CT) and Magnetic Resonance Imaging (MRI), have been used for soil investigations. MRI allows complex insights into the processes occurring within the porous medium. It has been used for tracing the water within the sample (VOTRUBOVÁ *et al.* 2003), detecting the flow process during the infiltration-outflow experiments (SNĚHOTA & CÍSLEROVÁ 2005), estimating the temporal changes of the water content during the infiltration experiment within undisturbed heterogeneous soil samples in 1D or 2D MRI (AMIN

et al. 1997; VOTRUBOVÁ *et al.* 2003), investigating the transport processes with the use of various tracers (HERRMANN *et al.* 2002a; POHLMEIER *et al.* 2008), and many others. Above that, 3D imaging can be done (POSADAS *et al.* 1996; HERRMANN *et al.* 2002a, b). In the study published by BAUMANN *et al.* (2002) the flow velocity in larger pores, diffusion of water, and preferential flow paths were directly measured in a packed column of seven distinct layers of natural sediments. A 3D rendering of the pore space was constructed to serve as an input data set for a numerical flow model.

Supported by Ministry of the Environment of the Czech Republic, Project No. SP/2e7/229/07 and by DBU – Deutsche Bundesstiftung Umwelt.

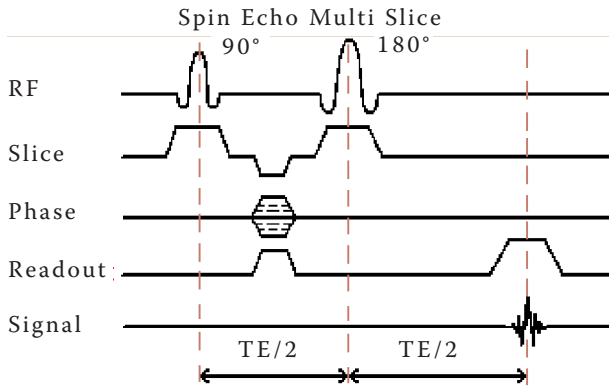


Figure 1. Spin echo multislice (SEMS) sequence diagram

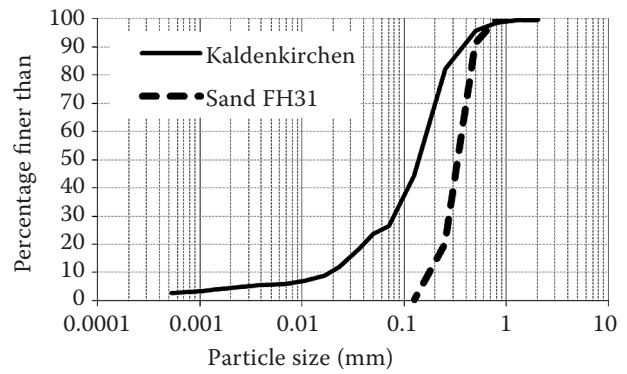


Figure 2. Grain-size curves of the soils under study

The main objective of the exploratory research presented is the evaluation and comparison of the vertical components of the velocity fields resulting from dripping irrigation. The measurements were done with two packed samples of different structures by means of 2D MRI. The flow of water and the propagation of a pulse of the $\text{Ni}(\text{NO}_3)_2$ tracer were monitored. Also the effects of two consecutive tracer pulses were imaged with the aim of testing the potential influence of different solute concentrations on the signal intensity of the adsorption power.

MATERIALS AND METHODS

The measurements were done on 7 Tesla vertical magnet system with a 40 mm RF probe. Flow experiments were monitored by the spin echo multi slice (SEMS) sequence shown in Figure 1. The MRI system employed is suitable for the use of Plexiglas cylinders of the outer diameter limited up to 40.0 mm. A set of tracer-infiltration

experiments was performed on two 120 mm high Plexiglas cylinders of 30 mm inner diameter filled with packed homogeneous sand (FH31) and packed with the composite sand-soil (FH31, Cambisol) configuration, respectively.

Frechen quartz sand (FH31) is a commercial product with standardised values of its chemical and physical characteristics and with a high chemical purity. The SiO_2 content is higher than 99% (www.quarzwerte.com). A periodically manured loamy sand (Gleyic Cambisol) was sampled at Kaldenkirchen, Germany. The soil samples taken from the ploughed topsoil horizon (Ap) were sieved (2 mm) and air-dried. In Figure 2, the grain-size analysis is shown using the dashed dark curve for the sand FH31 and the solid black line for the Cambisol soil (Kaldenkirchen). Just one vertical central slice of the sample is of interest (Figure 3), the parameters being given in Table 1. The y-axis in all images denotes the vertical direction and the x-axis the position of a particular vertical within the sample.

The infiltration was provided through a dripping system consisting of HPLC pump, non-compressible

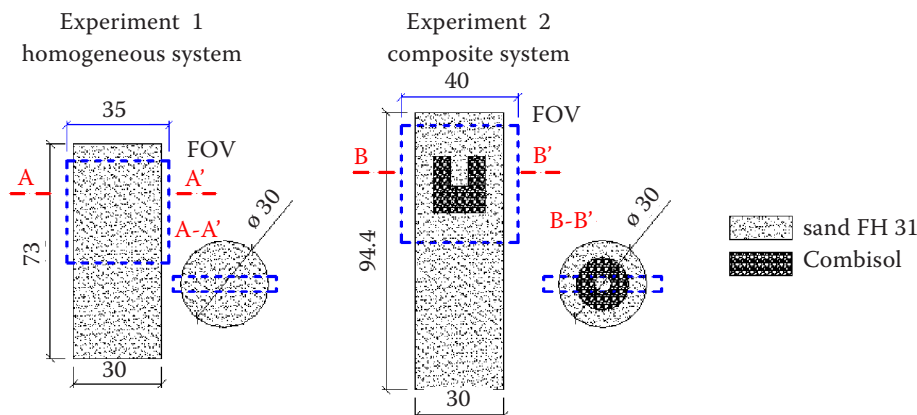


Figure 3. Illustration of the sample composition in Experiment 1 on the left and in Experiment 2 on the right (marked in mm)

Table 1. The basic MR-settings for Experiment 1 and Experiment 2

	TR (ms)	TE (ms)	Data matrix	Pixel size (mm)	FOV (mm)	Slice thickness (mm)	AT (s)
Experiment 1	100	1.23	64 × 64	0.55	35 × 35	5	51
Experiment 2	100	1.34	64 × 64	0.63	40 × 40	5	51

TR – repetition time; TE – time to echo; FOV – field of view for 2D vertical slices; AT – acquisition time

tubing, and the dripping head. The injection was arranged in such a way as to keep the HPLC pump system placed at a safe distance from the magnet. The dripping head was constructed as a one-point centric source unit, so the drops fell at the midpoint on the top of the sample. The uniform distribution of the infiltrating liquid was achieved by a thin highly permeable support plate placed on the top of the soil sample, thus the hydraulic contact was guaranteed. The tracer experiments were performed with a solution of nickel nitrate $\text{Ni}(\text{NO}_3)_2$ in a concentration of 0.05 mol/l. Identically, the tracer was added to the dripping system outside the magnet, reaching the top of the sample in the form of drops. The tracer progression was monitored by its effect on the signal relaxation of ^1H .

Two different experiments were designed and performed. The first one mapped the tracer transport within a homogeneous system (Experiment 1), the second one the transport within a composite sand-soil system (Experiment 2). One minute scanning time step was chosen in both cases.

Experiment 1

In Experiment 1 the sand FH31 was packed carefully into the Plexiglas cylinder to the height of 73 mm (Figure 3). Table 1 shows the MR-settings for Experiment 1. Initially, the sample was fully saturated. The dripping irrigation started right after the setting of a sample into the magnet. The HPLC pump was set to produce a flow rate of 0.5 ml/min. For infiltration, deionized (DI) water of pH = 3.5 was used. When the steady state condition was achieved, one ml of 0.05 mol/l $\text{Ni}(\text{NO}_3)_2$ solution of pH = 3.8 was injected into the pump tubing system as a tracer pulse without interrupting the infiltration run. Six minutes after the pulse application the tracer front appeared in the area of interest defined by the dimensions of the pre-selected field of view (FOV) (details in Table 1).

The tracer drained away approximately 22 min after the pulse application.

Experiment 2

In Experiment 2, the column was filled to the height of 94.4 mm. The porous media was formed as a composite of the sand FH31 and Cambisol. For Cambisol, a bowl of U-shape was chosen to create a basin inside the sand body, see Figure 3. The U-shape was assumed to act as a funnel to concentrate the flow into the Cambisol part of the composite sample. The design was tested in a series of previous experiments not discussed here. Table 1 summarises the main MR-settings for Experiment 2. Similarly to Experiment 1, the sample was fully saturated in advance. The HPLC pump for Experiment 2 was set to produce a flow rate of 0.5ml/min. For infiltration, deionized (DI) water of pH = 3.5 was used. Two tracer pulses of the solution were added during the continuous infiltration. The first pulse with pH = 3.8 and the second one with pH = 6.0 were injected under the steady state conditions with a 30 min interval. After 30 min from the injection, the first pulse was assumed to be completely washed out from the column. The continuous infiltration was stopped 70 min after the MR-acquisition had started. The start of MR-acquisition did not correspond to the start of the infiltration; to cover the steady state infiltration stage, it was delayed for about 20 min.

For the data analyses, an IDL-Routine for the velocity field calculation was adapted after HERRMANN *et al.* (2002a). The signal distribution of the tracer along a particular vertical is supposed to be Gaussian. The smoothed raw data for each time step and each vertical were thus fitted with the Gauss function, as shown in Figure 4. The vertical component of the flow velocity at each time interval was calculated as a distance between

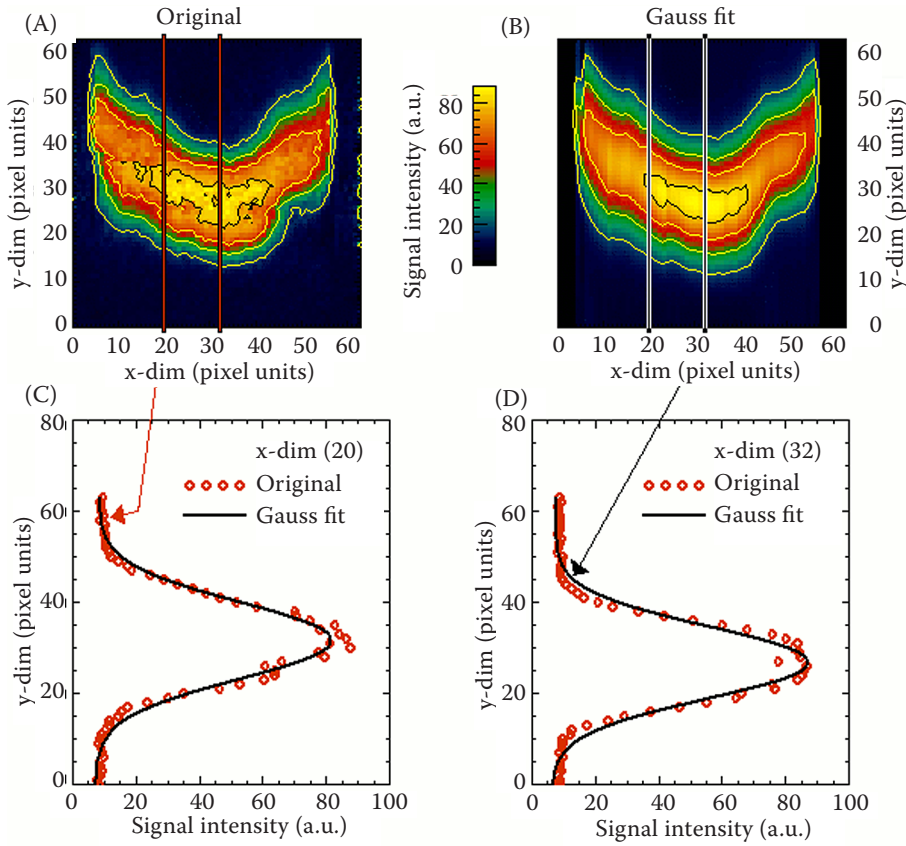


Figure 4. Data processing for the velocity field calculation, an example for 2D image at time t7 (compare to Figure 6). The original data of the 2D image of the tracer pulse at time t7 are displayed with marked column position (20, 32) in (A); the fitted data of 2D image of the tracer pulse at time t7 are displayed with marked column position (20, 32) in (B); the original data (red round symbols) and the fitted data (dark solid line) are plotted for the pointed verticals, x-dim (20) (C), x-dim (32) (D)

the two consequent positions of the Gauss peak along the vertical divided by the corresponding imaging pace, see Eq. (1).

$$v_y = \frac{\Delta y}{\Delta t} ; \Delta y = y_{T(i)} - y_{T(i+1)} ; \Delta t = T_{(i+1)} - T_{(i)} \quad (1)$$

where:

- Δy – vertical distance between the peaks positions (mm)
- Δt – time between the consequent image acquisitions (min), in this case the pace is regular, equal to one minute

In Figure 5 the graphical explanation is given. The described calculation results in a field of vertical components of local flow velocities. The results are shown in Figure 11.

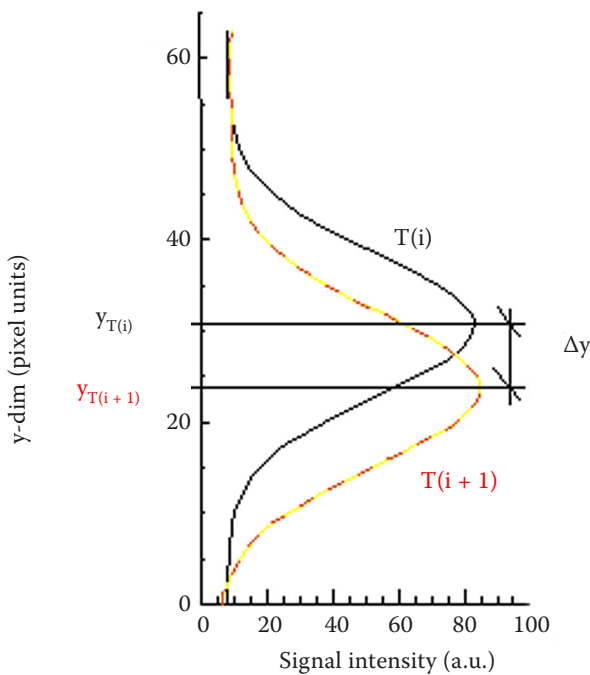


Figure 5. The principle of velocity field calculation; the nomenclature is identical to that in Eq. (1)

RESULTS AND DISCUSSION

Before the start of the tracer application a background (BG) image was taken to illustrate the steady state flow structure within the particular soil sample. For Experiment 1, a schematic diagram of $Ni(NO_3)_2$ progress is shown in Figure 6. The points in the sample (pixels) where the tracer propagation started to be disturbed are marked in the zoomed pictures. It is evident that the measured signal was

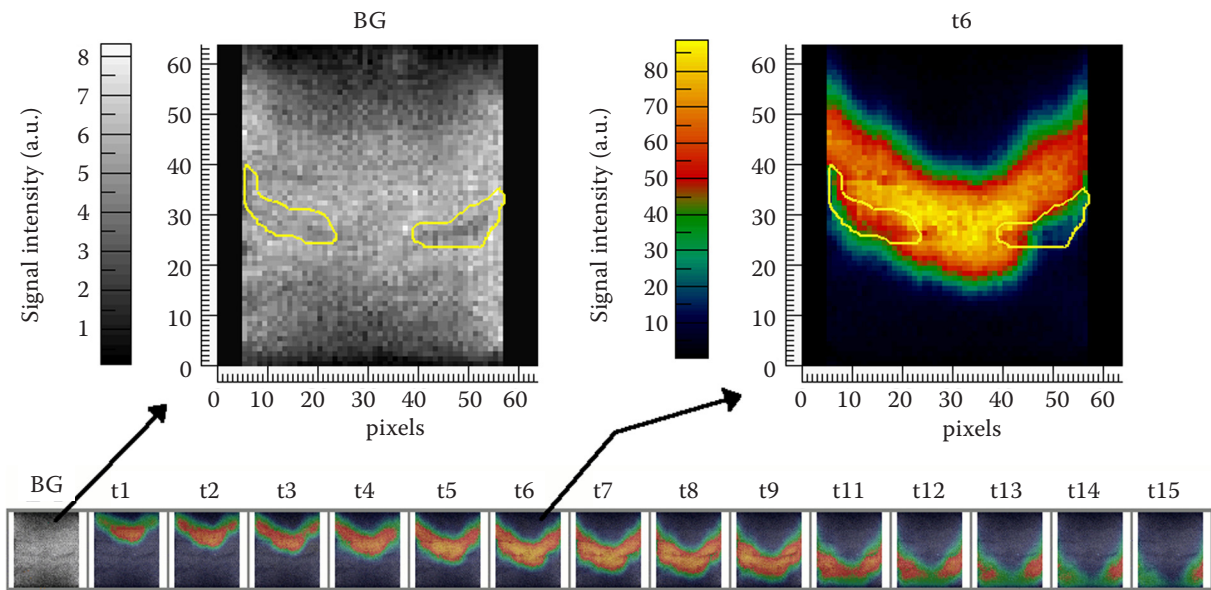


Figure 6. Experiment 1 – the illustration of the progress of the pulse motion within the sand FH31; in the background image (BG), enlarged on the left, two selected zones of disturbed structure are marked; the BG image was taken before the pulse application, when quasi-steady state flow had been reached; the impact of the disturbed structure on the pulse movement is apparent in the zoomed image t6; the row of images below describe the pulse motion during times t1–t15 (time gap at time t10 is due to the software problems)

weaker and, compared to the undisturbed locations, the propagation front became irregular (details in Figure 7). The shape of the tracer plume can be interpreted as a result of the centric, one-point dripping system. In this case uniform distribution of the infiltrating liquid was not achieved. The shape of the tracer plume cannot be explained by the faster solute progress in the middle part of the sample, which is clearer, compared to the map of local velocities in Figure 8. The darker coloured points (blue) in Figure 8 represent the locations with a faster solute progress. The basic statistics for the velocity field in Experiment 1, namely the mean value (1.7 mm/min), the variance (0.52 mm/min), and the mean absolute deviation (0.45 mm/min), are summarised in Table 2.

Table 2. The statistics of the velocity fields in Experiment 1 and in Experiment 2 (mm/min)

	Mean	Variance	Mean absolute deviation
Experiment 1	1.7	0.52	0.45
Experiment 2	1.4	0.82	0.7

Experiment 2 was intended to assess the changes of the signal response, the result of the impact of a real soil body placed inside the sand sample. The results of the conservative transport given in Figure 9 demonstrate the tracer propagation (pH = 3.8) within the composite sample. The left slice labelled BG illustrates the background signal coming from the composite sample. The higher signal intensity values originate from the Cambisol body, especially from the parts apparently disturbed during the sample preparation. The disturbed domains create preferential pathways for the flowing solute.

In Figure 9, the neighbouring slices at the times, labelled t7 and t10, indicate the locations influenced by the tracer at specific times, 7 and 10 min, after the pulse appearance in the FOV. Despite a favourable bowl shape, the flow largely bypassed the Cambisol body due to the contrasting hydraulic characteristics of the two soil materials used. The detailed image analysis revealed pixels within the Cambisol body that were marked by the passing tracer. The affected pixels from the Cambisol part formed a breakthrough path for the infiltrating solute, the tracer flowing preferentially through the large voids. It may be possible

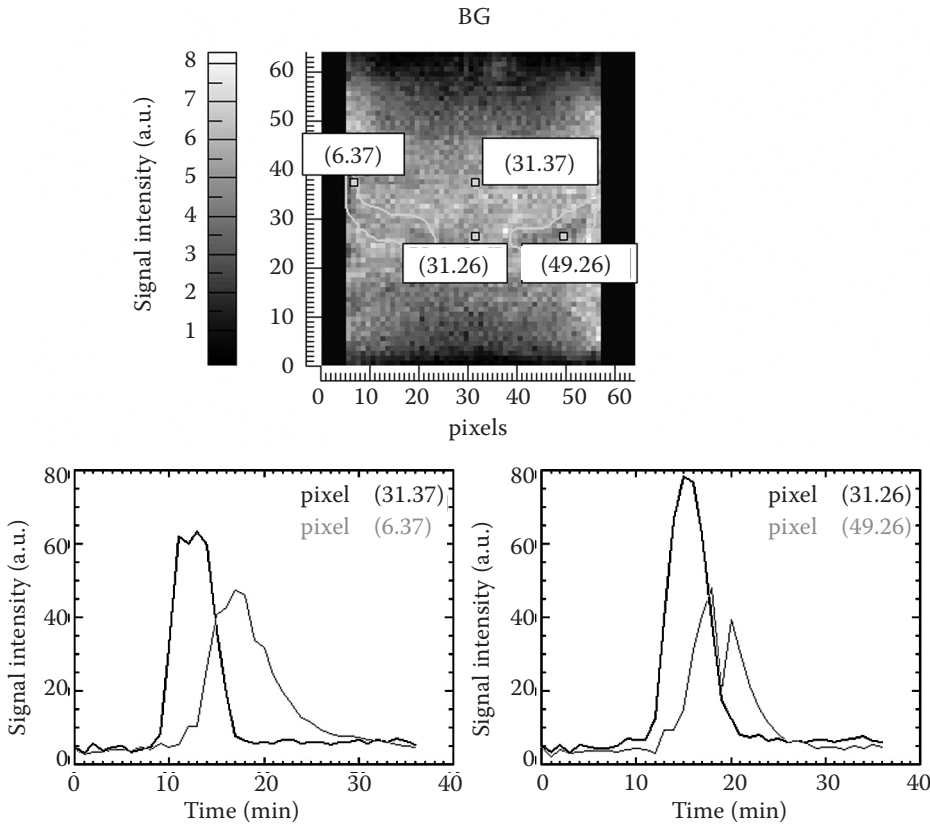


Figure 7. Experiment 1 – the changes of signal intensities of four selected pixels are plotted in time; on the left, two pixels of equal depth (\approx layer 37) are shown; two pixels of the depth corresponding to layer 26 are on the right, the pale grey line demonstrates the tracer propagation in zones of disturbance (position see above); the dark line depicts the signal intensities in the pixels located in the middle part of the sample with no visible structure disturbance; in both cases, the tracer pulse reached the disturbed zones with a delay, with lower peaks and extended appearance; the reason for the double peak appearance is unexplained

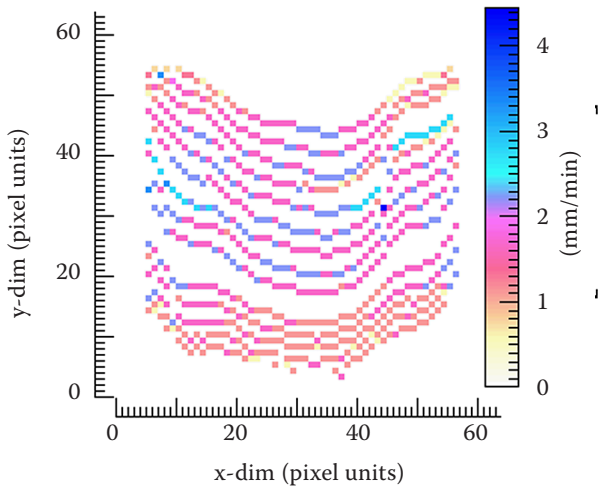


Figure 8. The velocity field in Experiment 1; the missing velocity values in the lower part of the velocity field are the results of technical problems with the software used for MRI

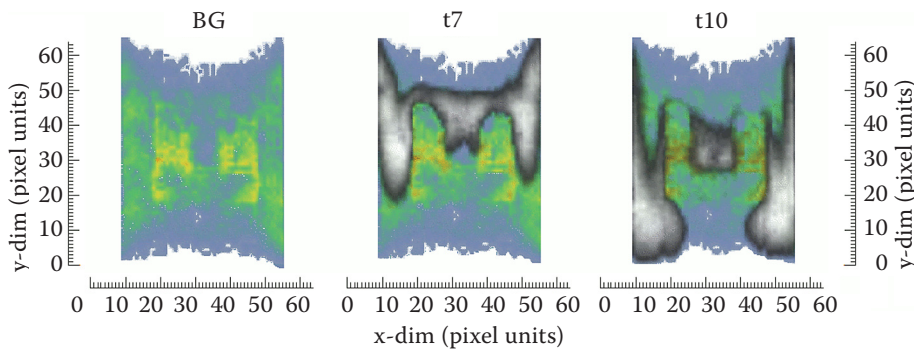


Figure 9. Tracer pulse motion within the composite system at three different times, before the pulse application BG and at 7 and 10 min after the pulse appeared in the FOV

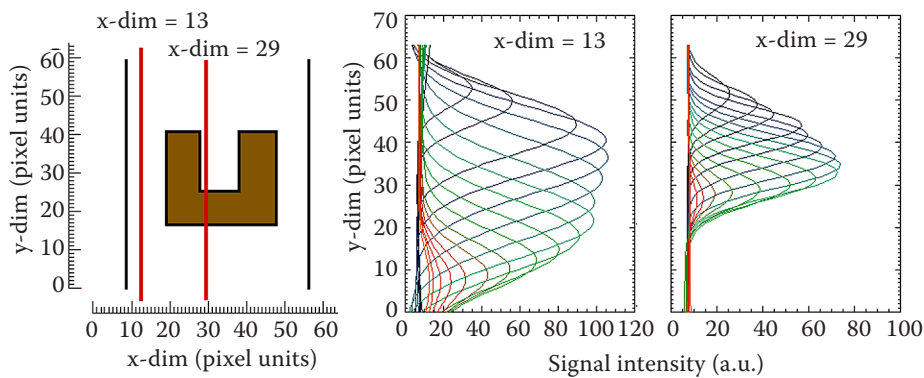


Figure 10. Temporal changes of the signal intensity plotted along vertical lines $x\text{-dim} = 13$ and $x\text{-dim} = 29$; the colour scale from dark blue to red corresponds to the individual times, e.g. the darkest blue corresponds to time t_1 , the middle-green to time t_7 , and the red colour to time t_{17}

that such voids were formed during the manual sample filling.

The plot on the left hand side of Figure 10 depicts the temporal changes of the signal intensity along the vertical line $x\text{-dim} = 13$ which passes through the sand FH31 only and does not cross the Cambisol zone. The plot on the right hand side of Figure 10 represents the temporal signal intensity changes along the vertical line $x\text{-dim} = 29$, which lies in the central part of the sample and crosses the bottom of the U-shape of the Cambisol body. In this vertical, the Cambisol material did not produce any signal at all. Evidently, the solute found some preferential pathways through this zone diverting this vertical (note Figure 9).

The vertical flow velocity field for Experiment 2 ($\text{pH} = 3.8$) was calculated. The velocities are depicted in Figure 11. The flow was slower at the interface between the two soil materials. It can be assumed that at this boundary, the vertical component of the flow lost its predominance and the horizontal component took over. This phenomenon can be explained by significantly different hydraulic characteristics. The material with a lower conductivity acts as a flow barrier.

In comparison with Experiment 1, the velocity field in Experiment 2 appears to be more heterogeneous, which is explicable considering the sample material arrangement. See the statistics for Experiment 2, the mean value (1.4 mm/min), the variance (0.82 mm/min) and the mean absolute deviation (0.7 mm/min), and compare these with the statistics of Experiment 1 in Table 2.

As mentioned in the previous chapter, in Experiment 2, with the aim of testing the potential influence of the different tracer pHs on the MR signal intensity, two consecutive tracer pulses were done in addition. According to some papers (HARTER 1983; ALTIN *et al.* 1999), the acidity of a

solute may have an impact on the tracer reactivity in the dependence on a certain pH threshold. The solutes with pH lower than this threshold are conservative, while a higher acidity leads to sorption. The temporal changes in the signal intensities at each point of the central vertical plane were thus studied consequently for two solutes of different pH values. For the lower pH value ($\text{pH} < 5$, in our case $\text{pH} = 3.8$), the transport may be considered as conservative, for the higher values as reactive (in our case $\text{pH} = 6.0$) (HARTER 1983; ALTIN *et al.* 1999).

The influence of the varying pH values of the applied tracer on the MR-signal intensity reflecting the flow of the solute is discussed below. The left plot in Figure 12 shows the signal intensity along the vertical line $x\text{-dim} = 13$, which is the boundary part of the sample where the flow goes just through the sand FH31. The dark solid line with symbols represents the first tracer pulse of $\text{pH} = 3.8$, the second lighter dashed line depicts the second tracer pulse of $\text{pH} = 6.0$. The plot on the

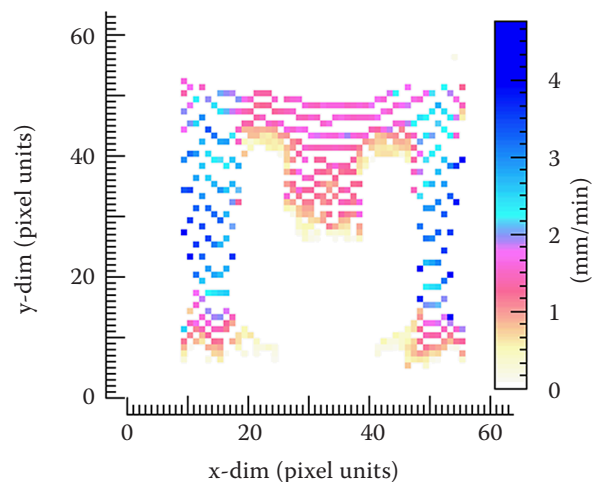


Figure 11. The velocity field in Experiment 2 ($\text{pH} = 3.8$)

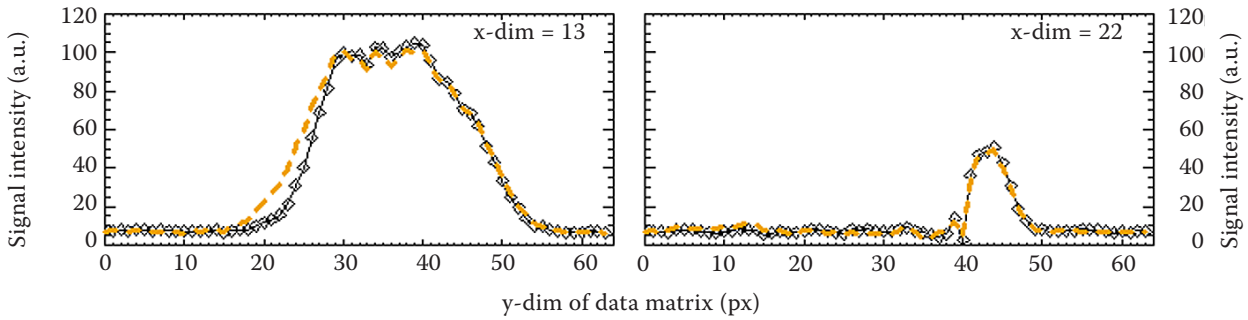


Figure 12. The influence of varying pH values of the tracer on the flow, on the MR-signal respectively (the vertical dimension is plotted along the horizontal axis); the dark solid line with symbols represents the first tracer pulse of pH = 3.8, the second lighter dashed line represents the second tracer pulse of pH = 6.0; the intensity values are plotted along two vertical x-dim = 13, x-dim = 22, respectively

right in Figure 12 shows the signal intensity along the vertical line x-dim = 22, which intersects both materials, the sand and the Cambisol. Both plots correspond to the time t7 (compare with Figure 9). Despite the manual performance of the experiment (hand-operated screening and pulse application), we obtained two well corresponding data sets. The courses of the shape and volume of both curves are in a good agreement. In some other verticals, the shape of the curve, i.e. the result of the second pulse, resembles the shape of the curve from the first tracer pulse, but the volume (integral) differs slightly (the left plot in Figure 12). Changing the structure of the porous media or some effects of the air dissolution could be a possible reason. In the studied case, the range of the varying pH value of the tracer seems to have no significant effect on the signal intensity within the sand FH31.

By assessing the variation in maximum differences of the signal intensities at each point

(pixel) during the two tracer pulses experiments, we obtained the maps of the domains which were more or less affected by the passing tracer/flow (Figure 13a, b). Subsequently, the two consecutive tracer pulses experiments were compared by simple subtraction (a) – (b) (Figure 13c). For each point in Figure 13a, the value was calculated as a difference between the background signal intensity and maximum signal intensity reached following the first tracer application breakthrough at this point. The background signal intensity value is the value that corresponds to the signal intensity during the steady state infiltration experiment as measured before the tracer application. An analogous calculation was done for the second application of the tracer, Figure 13b. The difference between 13a–13b is shown in Figure 13c in which the green colour represents the pixels with no change in signal intensity between the two tracer runs. On the other hand, the red and blue

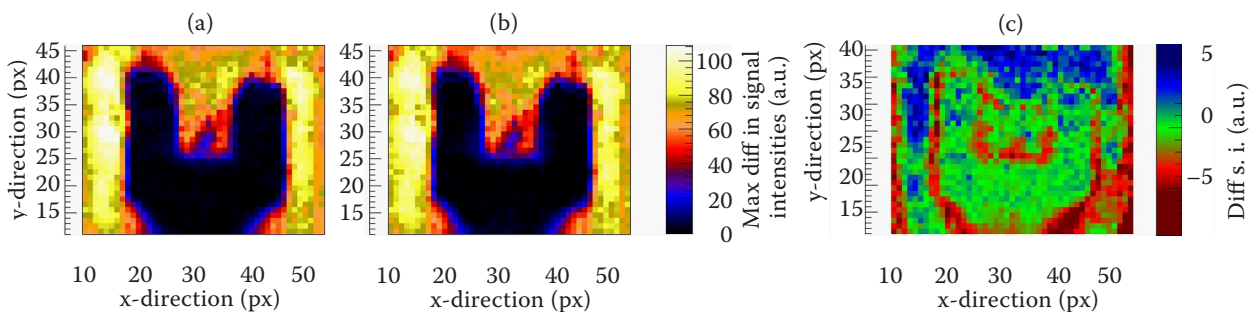


Figure 13. The influence of the pulse breakthrough on each pixel. For (a) (b) figures – the lighter is the pixel, the more it was affected by the flow/transport; the (a) case corresponds to the first pulse application (pH = 3.8), the (b) case to the second pulse application (pH = 6). On (c) is shown the difference map of signal intensities between the two pulses for each pixel. The green colour (zero value) presents the pixels with no changes in the signal intensity between the two tracer’s applications

colours depict the pixels with a marked difference between the two tracer applications.

CONCLUSIONS

The flow velocity field was evaluated in the tracer-infiltration experiments performed on a sand column sample and on a system of sand-Cambisol composition. Small disturbances in the tracer front propagation were observed during the breakthrough in both cases. Only the vertical component was calculated for the velocity field. This simplification suits better the homogeneous sample, where the variation of the velocity value was lower than in the case of the composite system. These small disturbances can be related to the way of the sample packing resulting in the preferential flow phenomena possibly in combination with air bubble entrapment. With the composite system, the flow was not predominantly vertical on the interface between the soils layers but the horizontal component significantly influenced the velocity field (note the velocity field in Figure 11). The U-shape body of Cambisol acted as a flow barrier. Infiltrating solute tried to pass by this barrier and found preferential pathways along the layer interfaces and disturbances within the Cambisol body.

The influence of the varying pH value of the $\text{Ni}(\text{NO}_3)_2$ tracer was investigated in the case of the composite sample. No remarkable changes occurred with the sand FH31 in the signal intensity coming from the first pulse of pH = 3.8 in comparison to the signal intensity resulting from the second pulse of pH = 6. This finding is in a good agreement with the adsorption isotherm measurement, where no adsorption was monitored for the sand FH31. In the case of Cambisol, a weak adsorption was measured at higher pHs (adsorption isotherms were performed in the FZ Jülich). For the selected range of pH in both cases studied, the tracer acidity did not influence the measured MR signal intensity.

The presented project was designed as a preliminary work for future research. The small scale investigation used in this study was limited by the technical abilities of the research centre Jülich at the time. Further investigation has been done with respect to the findings by SNĚHOTA *et al.* (2008) focused on the assessment of the entrapped air. The study performed on large undisturbed sam-

ples implies the linear relationship between the quasi steady state flow rate and the entrapped air content.

The MRI technique serves as a good tool to study the flow and transport processes in soil. However, the need to improve the devices and investigatory methods is still enormous, especially as concerns undisturbed natural soils.

Acknowledgements. We thank the anonymous referee for helpful comments on the paper.

References

- ALTIN O., OZBELGE O.H., DOGU T. (1999): Effect of pH, flow rate and concentration on the sorption of Pb and Cd on montmorillonite: I. Experimental. *Journal of Chemical Technology and Biotechnology*, **74**: 1131–1138.
- AMIN M.H.G., CHORLEY R.J., RICHARDS K.S., HALL L.D., CARPENTER T.A., CÍSLEROVÁ M., VOGEL T. (1997): Study of infiltration into a heterogeneous soil using magnetic resonance imaging. *Hydrological Processes*, **11**: 471–483.
- BAUMANN T., PETSCH R., FESL G., NIESSNER R. (2002): Flow and diffusion measurements in natural porous media using magnetic resonance imaging. *Journal of Environmental Quality*, **31**: 470–476.
- HARTER R.D. (1983): Effect of soil pH on adsorption of lead, copper, zinc, and nickel. *Soil Science Society of America Journal*, **47**: 47–51.
- HERRMANN K.-H., POHLMEIER A., WIESE S., SHAH N.J., NITZSCHE O., VERECKEN H. (2002a): Three-dimensional Ni^{2+} ion transport through porous media using Magnetic Resonance Imaging (MRI). *Journal of Environmental Quality*, **31**: 506–514.
- HERRMANN K.-H., POHLMEIER A., GEMBRIS D., VERECKEN H. (2002b): Three-dimensional imaging of pore water diffusion and motion in porous media by nuclear magnetic resonance imaging. *Journal of Hydrology*, **267**: 244–257.
- POHLMEIER A., VAN DUSSCHOTEN D., WEIHEMÜLLER L., SCHURR U., VERECKEN H. (2008): Imaging water fluxes in porous media by magnetic resonance imaging using D_2O as a tracer. *Magnetic Resonance Imaging*, **27**: 285–292.
- POSADAS D.A.N., TANNÚS A., PANEPUCCI H., CRESTANA S. (1996): Magnetic resonance imaging as a non-invasive technique for investigating 3-D preferential flow occurring within stratified soil samples. *Computer and Electronics in Agriculture*, **14**: 255–267.

SNĚHOTA M., CÍSLEROVÁ M. (2005): Infiltration outflow experiment monitored by means of magnetic resonance. *Journal of Hydrology and Hydromechanics*, **53**: 54. (in Czech)

SNĚHOTA M., SOBOTKOVÁ M., CÍSLEROVÁ M. (2008): Impact of the entrapped air on water flow and solute transport in heterogeneous soil: Experimental set-up. *Journal of Hydrology and Hydromechanics*, **56**: 247–256.

VOTRUBOVÁ J., CÍSLEROVÁ M., AMIN M.H.G. , HALL L.D. (2003): Recurrent ponded infiltration into structured soil: A magnetic resonance imaging study. *Water Resources Research*, **39**: 1371.

Received for publication March 5, 2009

Accepted after corrections October 27, 2009

Corresponding author:

Ing. VLADIMÍRA JELÍNKOVÁ, České vysoké učení technické v Praze, Fakulta stavební, katedra hydromeliorací a krajinného inženýrství, Thákurova 7, 166 29 Praha 6-Dejvice, Česká republika
tel.: + 420 224 353 725, fax: + 420 233 337 005, e-mail: vladimira.jelinkova@fsv.cvut.cz
